Journal of Polymers and the Environment
https://doi.org/10.1007/s10924-024-03368-5

ORIGINAL PAPER

Structure Development in Cross-Linked, Soybean Oil-based Waterborne Polyurethanes

Zoran S. Petrović[1] · Jasna Djonlagić[1] · Jian Hong[1,2] · Milica Lovrić Vuković[1] · Jan Ilavsky[3] · Brian G. Bush[4] · Fan Zhang[4]

Accepted: 24 July 2024

Abstract

Development of waterborne polyurethanes (WPU) using bio-based sources represents a step towards sustainable materials science and industry. We synthesized bio-based cationic water-dispersed crosslinked polyurethanes from high oleic soybean oil (HOSO) polyol, isophorone diisocyanate, and methyldiethanol amine, with varying ionic group contents after neutralization with acetic acid. Our primary objective was to analyze how crosslinking affects the dispersion process and film properties in multifunctional systems. The synthesis-structure-property relationship is elucidated through comprehensive analyses of the products at different stages of the synthesis. The dispersion of the WPU particles in water must occur prior to gelation during the final preparation, leading to incomplete conversion and the formation of imperfect networks. Insight into the synthesis process and polymer structure was gained by simulating polymer network parameters. Morphological analyses using synchrotron-based X-ray scattering and atomic force microscopy revealed a hierarchical structure within the WPU films. Importantly, all the films prepared in this study, without using coalescence agents, have low water absorption and high water contact angles, demonstrating their potential for textile and leather coatings and other applications.

Graphical Abstract

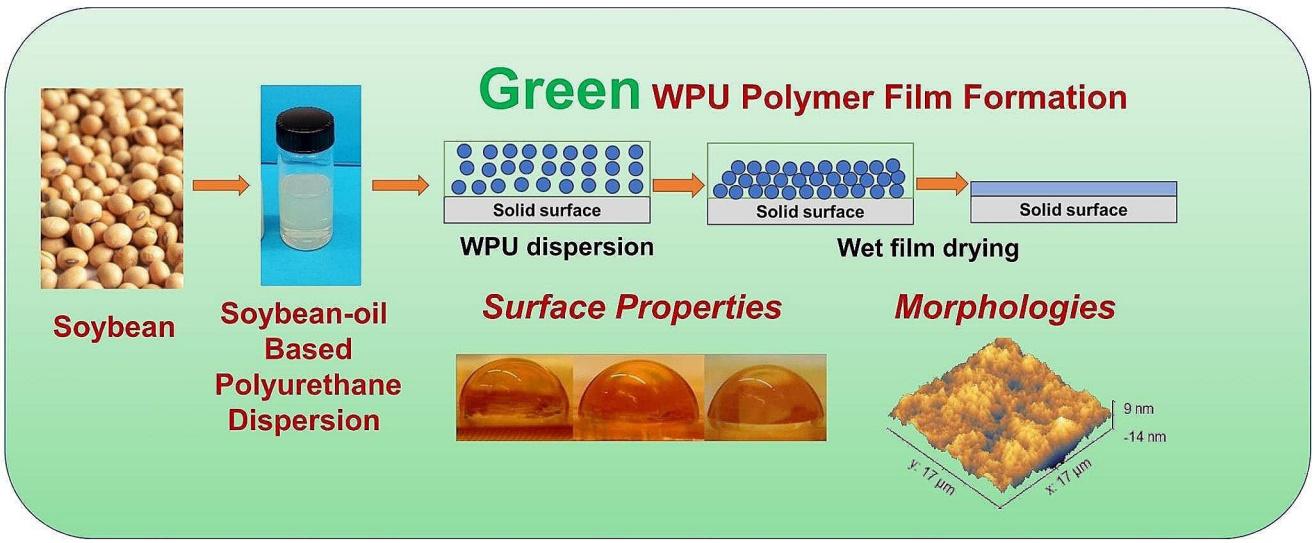

Keywords High Oleic Soybean oil · Cross-linked Polyurethane · Waterborne Polyurethanes · Bio-based Polymers · Renewable Polymers · Sustainable Materials

Extended author information available on the last page of the article

Published online: 16 August 2024

Introduction

Environmental concerns and green chemistry requirements demand the development of new coating materials for various applications. The new products should minimize the use of volatile organic compounds, utilize renewable raw materials, maintain high performance, and be cost-effective. Polyurethane dispersions (PUD) in water, derived from vegetable oils, are excellent candidates that meet all these requirements. These dispersions consist of nanometer- or micrometer-sized polymer particles, whose stability in water is offered by ionic groups that act as surfactants. These surfactants also allow the break-up of the polymerizing mass into small particles during preparation.

A seminal paper by Dieterich [1] described the fundamentals of PUD, including the mechanisms of polymer's formation and structure. The cationic polymers incorporate amines that are neutralized by low molecular-weight acids. The cationic dispersion's pH value is controlled by the neutralizing agent being acidic (pH < 7). Particularly, the cationic dispersions, such as those discussed in this paper, are frequently used in hydrophobization of textiles and leather. These polymers are amphiphilic containing hydrophilic ionic groups necessary to achieve good dispersion in water while the incorporation of oil-based soft segments and hydrophobic additives can enhance the material's water repellency. Using polyfunctional triglyceride polyols is more cost-effective and leads to crosslinked products with enhanced mechanical strength, durability, and thermal stability. Despite these advantages, polyfunctional polyols present challenges during polyurethane preparation, such as possible early gelation (dispersion in water must occur while the polymer system remains liquid). The reaction is finished in dispersed droplets of the remaining reacting mass. The critical question is determining the optimal conversion point for dispersing the system in water, an issue not addressed in the literature. The reaction between water and diisocyanate alters the stoichiometry of the components, leading to imperfect networks or even preventing network formation. To minimize this water-isocyanate reaction, the gel point should be shifted to a higher conversion. This can be achieved by using polyols with a functionality close to two, such as high oleic soybean polyol (SOP) mixed with the short diol (MDEA), and utilizing diisocyanate with unequal NCO group reactivity and a solvent. Polymerization is typically carried out until the reaction mixture reaches a certain viscosity, which also depends on the solvent concentration. Dispersion often occurs at an arbitrary time.

The only method to determine if a network has formed is by measuring the amount of the soluble fraction in good solvents. If a network has not formed, the sol fraction of the final polyurethane films will be 100%, while a perfect network will have a 0% sol fraction. The gelation study in this paper, based on branching theory, allows for calculating the conversion from the sol fraction. The success of the preparation process was quantified by simulating network formation and comparing it with experimental results.

Ionic polymers in dispersions are amphiphilic. A higher ionic group content improves the stability of water dispersions, balanced by hydrophobic oil soft segments to enhance the water contact angle. The success of film formation from water dispersions was compared with films made from melt casting of similar composition. The analysis also involved synthesizing the pure hard segment to observe the ultimate properties.

Polyurethane (PU) elastomers are characterized as two-phase systems, comprised of alternating soft and hard segments. [2] The phase separation and domain formation result from hydrogen bonding and differences in polarity between the hard and soft segments. These domains may be globular at low hard segment content, exhibit a co-continuous morphology when the soft and hard phases are present in approximately equal mass concentrations, or appear mixed at intermediate segment concentrations. [3–6]

The structure of hard segments and domains in the PUD films may be more complex than in typical PU elastomers, owing to different forces such as ion-ion interaction, ion-hydrogen bridges, and ion-dipole interactions, all of which may modify the morphology [7–9]. The utlization of vegetable oil adds a unique aspect to the polymer networks, due to the presence of dangling chains, specifically, parts of fatty acid chains do not contribute to load support in stressed samples, but instead act as plasticizers [10].

High-purity monomers are necessary for synthesizing high molar mass polymers, whereas natural raw materials, particularly vegetable oils, are known for their heterogeneity and various "impurities". High oleic soybean oil (HOSO), which features triolein as the major component and on average has three double bonds, provides a more uniform composition and enables better control of the structure and properties of polyols and polyurethanes. The analysis of polyurethane networks in cross-linked PUD systems and the subsequent comparison with calculated structures help to explain the defects during network formation and the associated degradation behavior of mechanical properties.

Although a wide range of diisocyanates can be used, aliphatic and cycloaliphatic ones are preferred, particularly isophorone diisocyanate and hydrogenated MDI (4,4′-diisocyanato dicyclohexylmethane). These types are significantly less reactive than aromatic diisocyanates and do not result in yellowing when exposed to sunlight. Isophorone diisocyanate, with its two NCO groups of different reactivity, allows easier prepolymer formation and leads to enhanced reaction control. The reactivity of the NCO group varies and depends

on the catalyst used: the primary group is more reactive with 1,4-diazabicyclo [2.2.2] octane (DABCO) as a catalyst, and the secondary group is more reactive with dibutyl tin dilaurate (DBTDL) or without an added catalyst [11–13]. The half-life of the isophorone diisocyanate (IPDI) - water reaction without a catalyst is ≈one hour. [14] Using polyfunctional polyols results in crosslinked polyurethanes and contributes to higher mechanical strength and modulus. In particular, the application of soybean polyols with different functionalities has been demonstrated to strongly affect the resulting polyurethane's mechanical properties. [15]

The dispersion of a liquid polymer solution is typically achieved by the gradual addition of water to the polymer mixture and through vigorous stirring, which leads to an emulsion in water. The viscosity of the system is regulated by the added solvent. Our experience suggests that a lower viscosity, preferably below 1000 mPa.s, results in smaller particle size upon dispersion. Aliphatic and asymmetric diisocyanates are rather unreactive, allowing preferential reaction with polyols. Since the molar masses of step-polymerization products depend strongly on the purity of reactants, molar ratio of components, side reactions, and the presence of solvents, high molar masses are typically not expected in linear polymers. The reported values for linear polyurethanes were often in the range of 20,000 to 30,000 g/mol, [16–18] or lower than expected [7], and around 80,000 for nonionic TPU based on IPDI/PTMO/butane diol [19]. The reported values of several hundred thousand should be approached with caution, due to analytical issues (poor solubility, agglomeration) or crosslinking.

Crosslinked PUD systems do not have such issues. For the successful dispersion, a polymer solution should have low viscosity, but no critical value can be specified since it depends on the shearing forces applied. It must be noted that low viscosity is necessary in the prepolymer process [20]. The polyols used in prepolymers have viscosities above 1000 mPa.s while the prepolymers themselves can have viscosity in the range of 5000-50,000 mPa.s. Nevertheless, incorporating a solvent can reduce the viscosity to below 1000 mPa.s.

High oleic soybean oil (HOSO) represents a new development opportunity for the soy and agriculture industry. Typically, HOSO comprises 75% oleic acid, 8% linoleic acid, and 12% saturated fats [21]. In this study, we used a commercially available HOSO having a slightly higher oleic acid content (see Supplemental Information) to prepare a polyol, which on average has three OH groups per triglyceride molecule. This research focuses on the usage of HOSO in polyurethane water dispersions and its impact on the structure-property relationships. To achieve this goal, we characterized the HOSO, epoxidized HOSO and the polyol in detail using chemical, spectroscopic, and physical methods to provide a comprehensive view and understanding of the structure of polyurethane networks. Specifically, we describe the network formation in cross-linked cationic polyurethanes with HOSO polyols, the preparation of water dispersions, the structure of the films and properties. Our morphological studies, combining surface-sensitive atomic force microscopy and the bulk X-ray scattering, aimed to gain insight into the complex structure of the final polyurethane films, which were derived from casting polyurethane dispersions in water.

Experimental

Materials

High oleic soybean oil, with an iodine value (I.V.) of 88.63 g I_2/100 g, was generously supplied by the Archer-Daniels-Midland Company[1]. Hydrogen peroxide (30 wt%in water), toluene (≥99.3%purity), glacial acetic acid (≥99.8%purity), and methyl ethyl ketone (MEK) were purchased from Fisher Scientific. Tetrafluoroboric acid (HBF4, 48 wt%in water), ion exchange resin Lewatite MP 64, and N−methyl diethanol amine (MDEA) (≥99%purity; M=119.2 g/mol) were obtained from Sigma Aldrich. Isophorone diisocyanate (IPDI) (98%, M=222.28; NCO% =37.8) was procured from Arcos Organic

Methods

Acid number was determined according to the IUPAC 2.201 standard. Hydroxyl number was measured using the P.A.P. method according to IUPAC 2.241. Epoxy oxygen content (EOC %) was assessed according to the ASTM D1652 Test method B by titration, using a standard 0.1 N perchloric acid in the presence of an excess of tetraethyl ammonium bromide. Viscosity was measured on a rheometer (AR 2000 ex, TA Instruments, New Castle, DE) using cone and plate geometry at 25 °C. Fourier Transform Infrared (FTIR) spectra were recorded on an ATR Perkin Elmer spectrometer (Spectrum Two, PerkinElmer, Waltham, MA). Size exclusion chromatography (SEC) was conducted on a system consisting of the Waters 515 pump (Waters Corp., Milford, MA), with a refractive index detector, tetrahydrofuran (THF) at 1 mL/min and a set of five Phenogel columns from

[1] Certain commercial equipment, instruments, or materials (or suppliers, or software,…) are identified in this paper to foster understanding. Such identification does not imply recommendation or endorsement by the National Institute of Standards and Technology, nor does it imply that the materials or equipment identified are necessarily the best available for the purpose.

Phenomenex (Torrance, CA) covering a molecular weight range from 100 to 5×10^5 g/mol.

Particle size and zeta potential were determined using the Zetasizer Lab Blue (Model: ZSU3100, Malvern Panalytical, Malvern, MA). The Ossila Contact Angle Goniometer was used to measure the water contact angle. Dynamic mechanical analysis (DMA) was conducted on a TA instruments DMA2980, in the tension mode at a heating rate of 3 °C/min and a frequency of 1 Hz. Atomic Force Microscope topographic images were captured using an Asylum MFP-3D AFM (Oxford Instruments Asylum Research, Santa Barbara, CA) operated in AC tapping mode. Differential scanning calorimetry (DSC) was performed on a DSC Q100 (TA instruments) at the heating rate of 10 °C/min under nitrogen. Thermogravimetric analysis (TGA) was evaluated on TA550 Discovery model (TA Instruments) at a heating rate of 10 °C/min under nitrogen (flow rate, 60 mL/min) up to 600 °C.

The WPU films were prepared by casting the WPU dispersions into a Teflon mold and drying them at room temperature for 2 days, followed by drying in an oven at 70 °C for 4 days. Approximately 1 mm thick WPU films were used for all further tests.

The degree of swelling and sol fraction were measured by placing ≈ 1 cm × 1 cm squares of the films in a glass jar containing 30 mL of DMF. The mass of the specimens was recorded until equilibrium (24 h for swelling and 48 h for sol fraction). The volume swelling degree was calculated using the formula Vs/Vo = [(Wo/ds) + (Ws - Wo)/dDMF] / (Wo/ds), where Vs, ds, and Ws are the volume, density, and mass (weight) of the swollen sample, respectively; Vo and Wo are the volume and mass (weight) of the initial sample, respectively; and dDMF is the solvent density.

The sol fraction is the mass of extracted soluble species from the swollen samples divided by the mass of the sample dried at 120 °C. Here, the sol fraction (%) is given by [(Wo - Wd) / Wo] × 100, where Wo and Wd represent the initial sample mass and the mass of the dried sample after swelling for 48 h, respectively. The swelling degree and sol fraction values were averages of 5 measurements.

X-ray scattering experiments using synchrotron-based small-angle and wide-angle X-ray scattering techniques were conducted on the ultra-small angle X-ray (USAXS) instrument at the 9-ID and another dedicated, fixed-energy instrument for small angle X-ray scattering (SAXS) and wide-angle X-ray scattering (WAXS) at the 12-ID, both at the Advanced Photon Source (APS), Argonne National Laboratory, U.S.A. The USAXS data were acquired at 21 keV, covering a continuous q range between $\approx 1 \times 10^{-4}$ Å^{-1} and ≈ 5 Å^{-1}. Here, the magnitude of the scattering vector $q = 2\pi/\lambda \sin(\theta)$, with λ and θ being the X-ray wavelength and one half of the scattering angle 2θ, respectively. Conversely, the 12-ID SAXS/WAXS data were acquired at 13.3 keV, covering a q range between $\approx 3 \times 10^{-3}$ Å^{-1} and 2.7 Å^{-1}. Both instruments have a similar flux density at $\approx 10^{13}$ photon/mm^2/s. More details about these instruments can be found elsewhere [22, 23].

The USAXS instrument, which operates in air, provides a broader q range for SAXS for polymer materials [24]. However, it has a lower signal-to-noise ratio compared to the 12-ID SAXS instrument where most of the beam path is in vacuum and reduces air scattering. Despite these differences in signal quality, both the USAXS and 12-ID SAXS results are consistent. Therefore, we will primarily discuss the data from the 12-ID SAXS instrument. We performed the measurements on cast WPU films with an approximate sample thickness of 1 mm.

Materials Preparation

EHOSO and Polyol Preparation

The preparation of epoxidized high oleic soybean oil (EHOSO) and the polyol (SOP) was conducted using the procedures detailed in the literature. [25–27] SOP was synthesized by ring-opening of epoxy groups with methanol.

At 100% conversion, epoxidized HOSO has a theoretical number-average molar mass (M_n) of 923 g/mol, an epoxy oxygen content (EOC) of 5.35% (experimental EOC was 4.97%), and an epoxy equivalent of 298.90 g/mol. The experimental conversion yield of epoxy groups was 0.93, which reduces the functionality to 2.87. The polyol viscosity at 25 °C was 1063 mPa.s, acid number was 0.22 mg KOH/g, and hydroxyl number was 151 mg KOH/g. A straightforward method to calculate M_n and functionality from the OH number is to match OH number with the calculated value obtained from the relationship between molar masses and the number of added OH and methoxy groups (M = 48), i.e., $M_n = 875 + 48f$, where 875 is the molar mass of HOSO and f is the functionality of the polyol. An OH number of 152 mg KOH/g corresponds to the functionality of 2.72 and molar mass of the polyol of 1005. The true M_n and the functionality are the average values and are somewhat higher due to the presence of oligomers. For practical purposes we have assumed that the SOP is a triol with a M_n = 1011 g/mol.

Preparation of Cationic Waterborne Polyurethane Dispersions

Five cationic polyurethanes were prepared from SOP, IPDI and MDEA, catalyzed by 0.1 wt% of dibutyltin dilaurate (DBTDL). The content of MDEA varied from 8.3 wt% to 12.5 wt%. SOP, IPDI and MDEA were charged in a 500 mL three-neck round-bottom flask equipped with a mechanical

Table 1 Designation and formulation of cationic water dispersions

Sample designation	SOP g	IPDI g	MDEA g	AA g	MEK g	H_2O g	Molar ratio OH_{SOP}/OH_{MDEA}	Molar ratio SOP/MDEA	HSC %
WPU-1	16.72	9.75	2.41	1.21	35	90	1/0.9	1/1.351	42.1
WPU-2	16.72	10.25	2.68	1.35	30	90	1/1	1/1.501	43.6
WPU-3	16.72	11.25	3.22	1.62	30	95	1/1.2	1/1.801	46.4
WPU-4	16.72	12.30	3.75	1.89	30	100	1/1.4	1/2.102	49.0
WPU-5	16.72	13.32	4.29	2.16	30	100	1/1.6	1/2.402	51.3

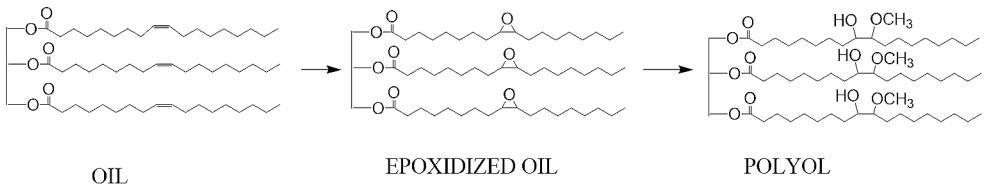

Fig. 1 Structure of HOSO, epoxidized HOSO and the SOP polyol

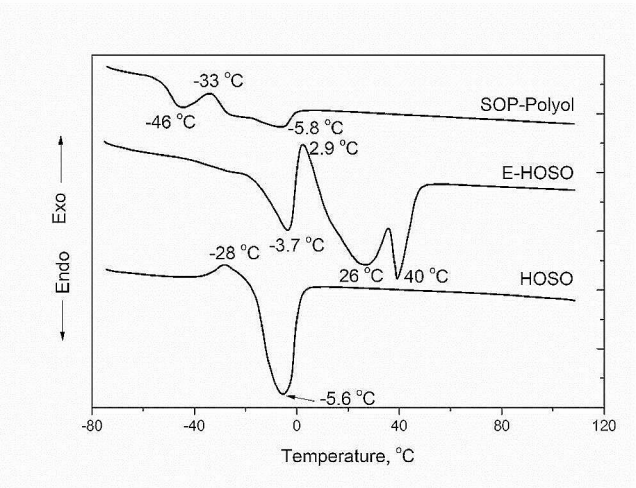

Fig. 2 The DSC data of HOSO, E-HOSO and SOP polyol

stirrer, reflux condenser, and nitrogen supply. The hard segment content (HSC) varied from 42.0 to 51.3%. The reaction mixture was stirred at 80 °C to 85 °C for 3 h with a gradual addition of solvent (MEK), then cooled to room temperature when the final portion of MEK was added. Neutralization with acetic acid (AA, 1.0 equivalents to MDEA) was achieved by stirring for 30 min, followed by emulsification in distilled water with vigorous stirring for 2 h, resulting in water dispersions. MEK was removed using a rotavapor at a temperature below 40 °C under vacuum. The total reaction time was 3 h. Table 1 summarizes the formulation and designation of the water dispersions. A slight excess of isocyanate, approximately 2% over the stoichiometric ratio, was employed.

Results and Discussion

Preparation and Characterization of the Soft Segment

We performed a comprehensive analysis of the products at each step of the synthesis, from the starting HOSO to the polyol (SOP) via epoxidized HOSO (EHOSO). Figure 1. Displays the structure of materials in each phase of synthesis.

HOSO, EHOSO and the polyol are pale yellow liquids, but EHOSO began to crystalize one day after its synthesis. DSC (first run) of HOSO, EHOSO and SOP, shown in Fig. 2, demonstrates their crystallization and melting behavior. Whereas HOSO shows a single melting peak at -5.6 °C, EHOSO displays peaks at -3.7 °C, a major broad peak at 26 °C and the highest at 40 °C which was tentatively assigned to the melting of epoxidized triolein. The polyol shows only a weak tendency for crystallization due to attached methoxy groups next to hydroxyls.

Figure 3a depicts the SEC curves for HOSO, EHOSO and SOP. The peaks for HOSO and EHOSO have very narrow mass distributions, while SOP has three distinct peaks at retention times of 22.2 min, 20.8 min, and 20.1 min, corresponding to the monomer, dimer, and trimer, respectively. The oligomer content in SOP was ≈12.1%. Notably, when HOSO undergoes epoxidation and becomes EHOSO, the resulting EHOSO peak slightly shifts to longer retention time, despite its higher molar mass. This shift is due to a more compact molecular coil. As expected, the hydroxylation process leads to SOP shorter retention times.

Figure 3b displays the FTIR spectra of HOSO, EHOSO, and SOP, respectively. During the epoxidation process, the double bound peak at 3005 cm^{-1} visible in the HOSO spectrum, completely disappears in the EHOSO spectrum. Simultaneously, the epoxy group is formed in EHOSO, evidenced by the emergence of a characteristic peak at

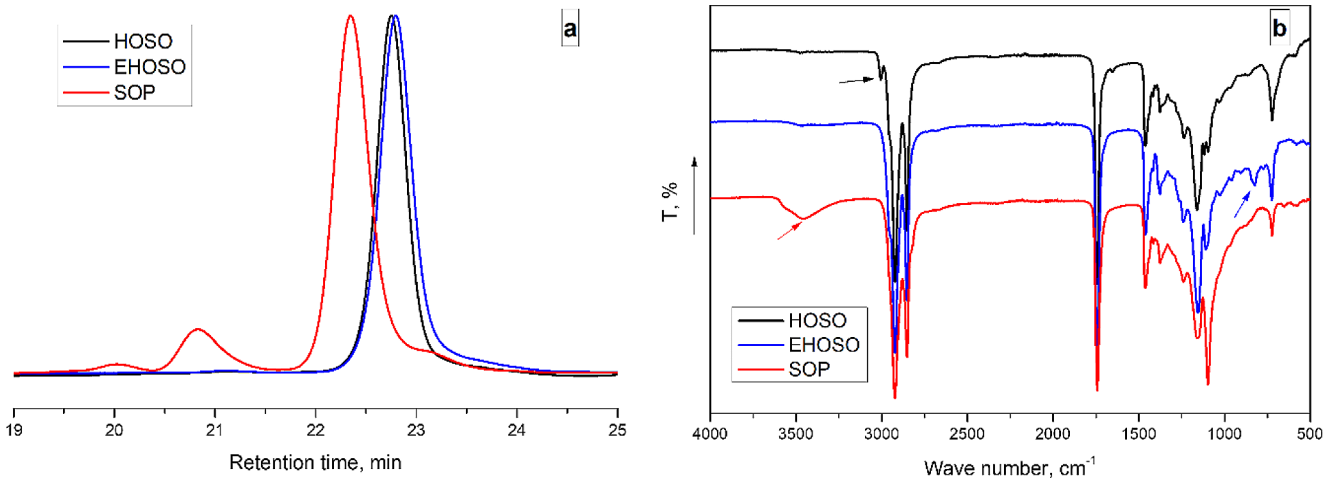

Fig. 3 SEC overlay of high oleic soybean oil (HOSO), epoxidized high oleic soybean oil (EHOSO) and SOP-polyol **a**, and their FTIR spectra **b**

825 cm^{-1}, confirming a high conversion from HOSO to EHOSO. In contrast, in the SOP spectrum, this epoxy group peak is absent, and the newly appeared broad band at approximately 3466 cm^{-1} indicates the formation of OH groups.

Scheme 1 illustrates the process of preparing dispersions from SOP, isophorone diisocyanate (IPDI) and MDEA to form cationic polyurethanes. These polyurethanes are subsequently neutralized with acetic acid

Various properties of five dispersions, such as their pH values, viscosities, zeta potential, and intensity-weighted (z-average) particle sizes, are reported in Table 2. The bio-based carbon content in PUs varied from 51 to 56%. The solid content of dispersions was kept constant at 24 mass %. These dispersions were acidic, with their pH monotonically increasing from 5.2 to 5.9 with increasing the weight% of MDEA and AA. An increase in the MDEA content also led to a slight increase in the viscosity of the dispersions, as well as improved stabilities and smaller particle sizes. While an empirical criterion for dispersion and emulsion stability is a zeta-potential value above 60 mV, [28] we found that it is not always precise for PU dispersions. For example, dispersions with an MDEA content greater than 10.3 wt% (and zeta potential ranging from 50 mV to 70 mV) showed no residue after centrifugation at 3000 rpm for 30 min. In contrast, those with lower MDEA content (WPU-1 and WPU-2) and zeta potential at approximately 60 mV showed a small amount of residue.

*Particle size; z-average; **a small amount of residue

The size distributions of the WPU dispersions are shown in Fig. 4. Its inset shows the images of the WPU dispersions. Evidently, with the increase in the MDEA content, the appearance of the WPUs changes gradually from milky white to transparent. This result indicates that a higher MDEA content leads to higher stability and reduces the probability of aggregation of the PU dispersion, consistent with the stability evidence following the centrifugation test. Particle size, as measured by Zetasizer using dynamic light scattering, ranged from 34 nm to 68 nm, following a general trend of higher the MDEA content leading to the lower particle size.

For simplicity, if we assume the WPU particles are spherical, the volume of a 40 nm particle is ≈33,510 nm^3. The particle mass was estimated to be 3.3×10^{-17} g, assuming a mass density of 1 g/cm^3. Considering that the repeating unit consists of one polyol unit (M ~ 1000 g/mol) and an equivalent mass of hard segments at 50% HSC from the mass balance, the repeat unit's mass would be 2000 g/mol. Consequently, each nanoparticle contains an estimated 10,000 repeat units. This value also represents the number of polyol molecules. For the dispersion to be stable, ionic species must be present on the surface of the particles to provide the required electrostatic repulsion. Given that the polyurethane is cross-linked and the whole particle is one molecule, the mobility of ionic groups is therefore restricted, affecting the zeta potential. The stability of the WPU dispersions, however, is complex. The large particles, with their larger surface area, allow more points of contact with particles, potentially leading to stronger van der Waals forces and promoting aggregation.

Preparation and Characterization of the Model Hard Segment

To understand the structure of the final polyurethanes and the interactions between the soft and hard segments, it is critical to investigate the properties of each type of segments individually. We have discussed the soft segment (polyol) in the sections above, and this section will be focused on the hard segment.

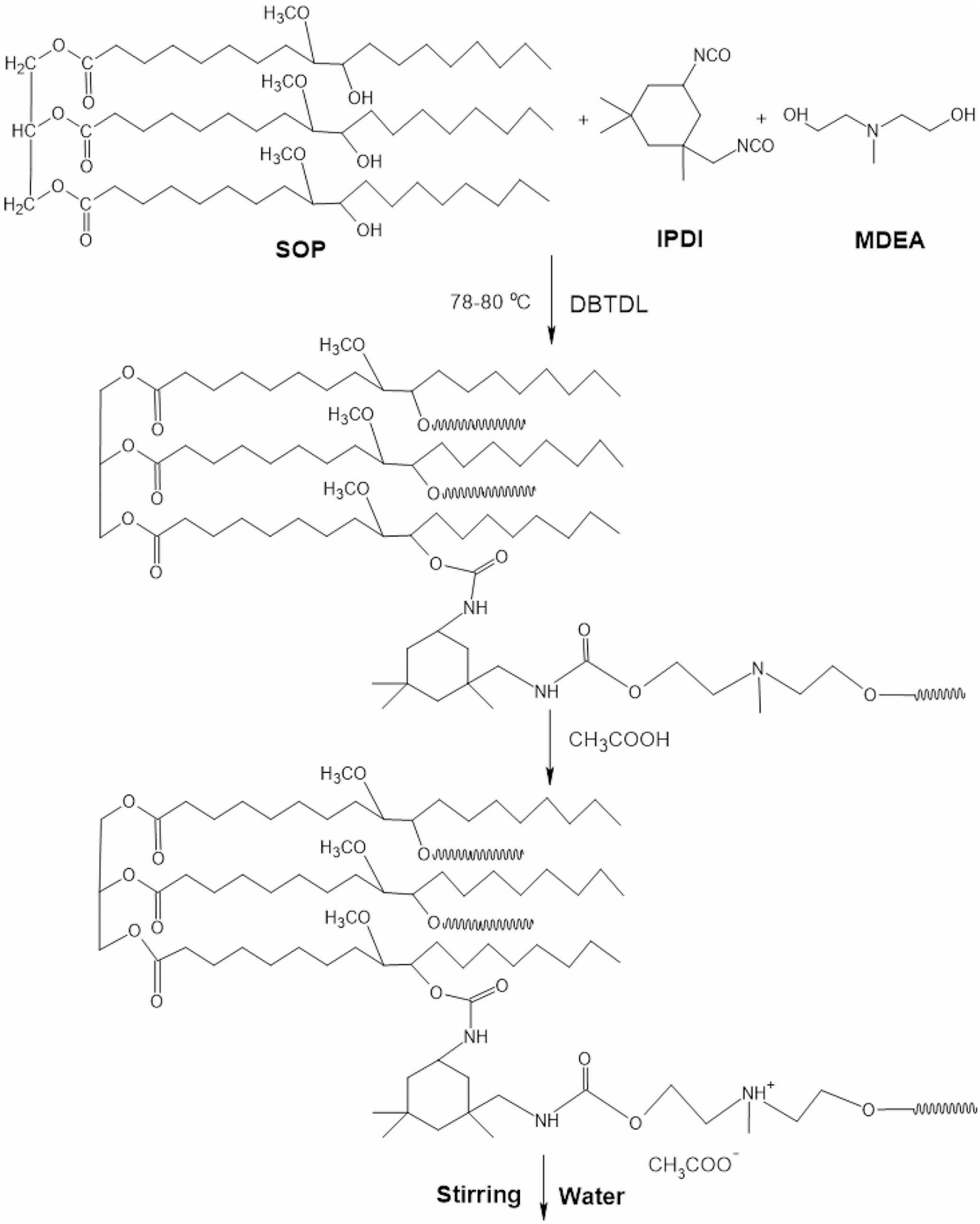

Scheme 1 The process for the preparation of waterborne cationic dispersions.

Table 2 Properties of WPU dispersions with different MDEA content. The MDEA stoichiometry, pH, solid content %, and viscosity are from single measurements

Sample	MDEA, wt%	pH	Solid content %	Viscosity mPas	Stability	Zeta potential, mV	*Particle size, nm (Polydispersity index)
WPU-1	8.3	5.2	24	6	**	60 ± 3.4	68 (0.444)
WPU-2	9.0	5.3	24	7	**	66 ± 2.8	63 (0.116)
WPU-3	10.3	5.3	24	8	stable	70 ± 2.6	48 (0.159)
WPU-4	11.5	5.6	24	13	stable	50 ± 2.6	34 (0.180)
WPU-5	12.5	5.9	24	11	stable	58 ± 0.9	38 (0.198)

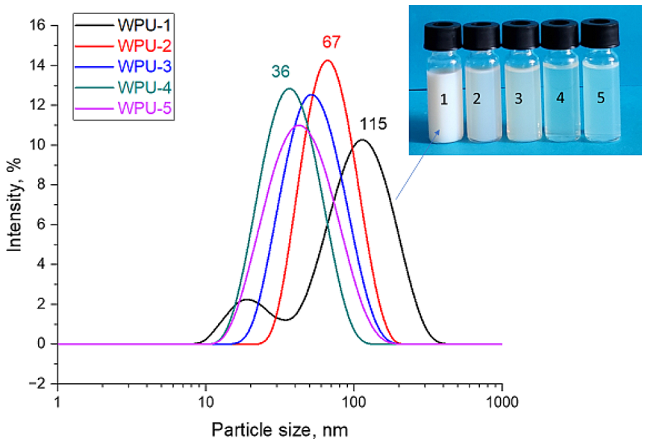

Fig. 4 Particle size distribution and the image of WPU dispersions with different MDEA contents. The values of 36 nm, 67 nm, and 115 nm, represent peak values. In contrast, the values reported in Table 2 represent z-average particle size

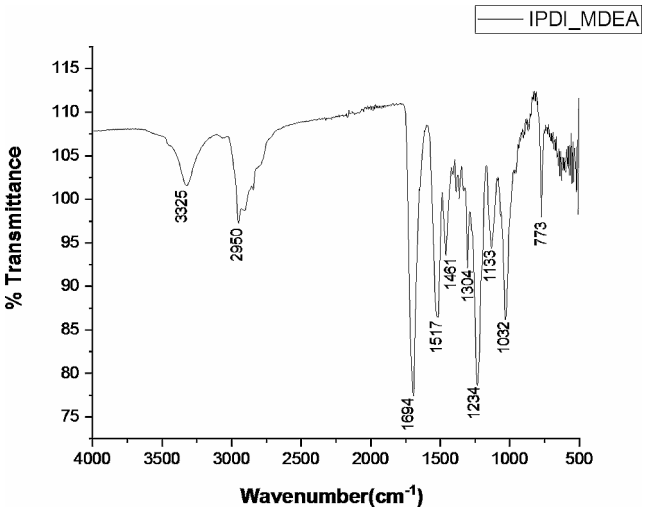

Fig. 5 FT-IR spectrum of pure IPDI/MDEA polyurethane

The hard segment, consisting of a polyurethane from IPDI and MDEA (as shown in Scheme 2), was prepared by mixing IPDI and MDEA at an equivalent molar ratio (see Supplemental Information). The resulting polymer was rubbery above 100 ºC, and became rigid and brittle upon cooling. Solubility tests reveal that this material is completely soluble in THF, methylene chloride, and chloroform; partially soluble in MEK; and insoluble in toluene and ethyl acetate. Surprisingly, it is also completely soluble in methanol, while remaining insoluble in water.

In essence, this model hard segment is an oligomer with a higher molar mass than that of the typical hard segments in the segmented PU used in this work. Efforts to isolate low molecular weight species by precipitation in water from the DMF solution were unsuccessful because it rapidly formed a milky dispersion even without neutralization with acetic acid. The size distribution in water showed a single distribution peak and the average particle size of 158 nm. The MDEA content in the polyurethane was 34.8%.

The ATR infrared spectrum obtained on powdered IPDI/MDEA polyurethane is presented in Fig. 5. N-H stretching band at 3325 cm^{-1} and carbonyl band at 1694 cm^{-1} are clearly visible, suggesting the presence of strong hydrogen bonds.

DSC analysis revealed the hard segment glass transition temperature of 77 °C and no melting peaks between − 100 °C and 200 °C, suggesting they were amorphous (see Supplemental Information). The asymmetric structure of IPDI and the presence of cis and trans stereoisomers are the primary reasons for the lack of crystallinity in these hard segments.

TGA analysis revealed a relatively low thermal stability of the hard segments (see Supplemental Information). We observed a rapid degradation starting at 220 °C, most likely due to the breaking of urethane bonds. The initial weight loss of ≈1% below 100 °C and an additional 2% weight mass leading up to 220 °C are likely due to the evaporation of absorbed moisture and retained acetic acid.

Scheme 2 The structure of the pure hard segment from IPDI and MDEA

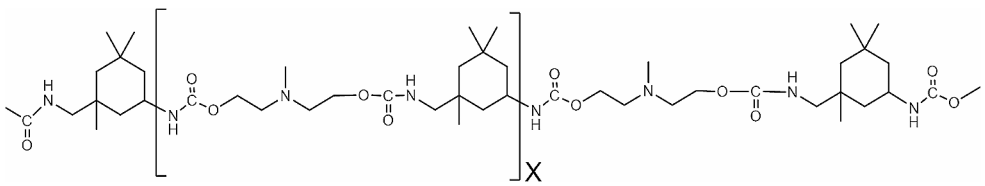

A pure soft segment would be the polyol itself minus the OH groups. The determination of the T_g of the soft segment is proven challenging. However, an IPDI/SOP polymer mixed in a stoichiometric ratio yielded a T_g at 7 °C, which is approximately 70 °C lower than that of the pure hard segments.

Characterization of the WPU Films

Structure and Morphology of Polyurethanes Synthesized using Soft and Hard Segments

The morphology of the cross-linked polyurethane networks is influenced by the hard segment length and concentration. Due to the differences in structure and polarity of segments, hard segments can form domains that can be globular at a low HSC and may become elongated or continuous at a high HSC. The chemical cross-links in the soft segments (trifunctional polyol) adds to the complexity. Scheme 3 illustrates the expected hard domain formation in the final polyurethanes due to the differences in polarity of the soft and hard segments, but the actual structure of domains in ionomers may be altered by the presence of stronger ionic and other interactions [8]. To characterize the microstructure, we employed AFM to provide a high-resolution and three-dimensional description of the surface topography and synchrotron-based high-sensitivity X-ray scattering to provide a bulk analysis of the atomic and meso-structures of the cast polymer films.

Scheme 3 Illustration of the domain structure in cross-linked polyurethanes with the IPDI/MDEA hard segments and the polyol soft segments

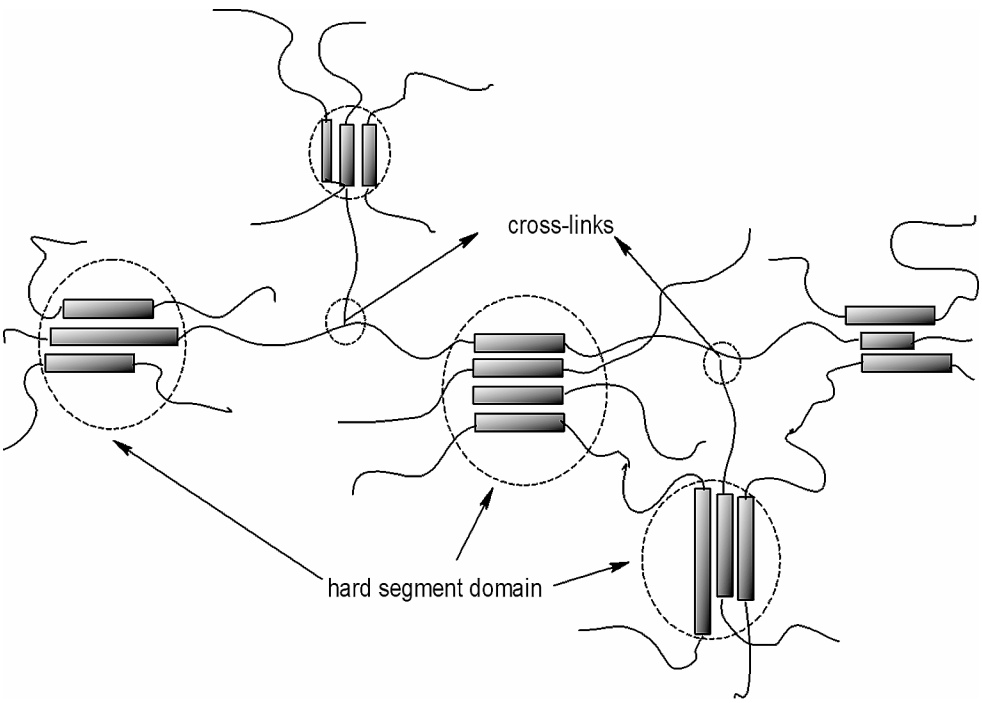

AFM Analysis of WPU Films

Topographic AFM analysis of the WPUs from SOP polyol exhibit an irregular, terraced or stacked layer structure as shown in Fig. 6**(a)** through **(c)**. The morphology of the films varied dramatically from that of previously investigated cast SOP/MDEA/IPDI films shown in Fig. 6**(d)** (described in Supplemental Information) which are smoother by comparison and do not form the terraced nanostructure. Figure 7**(a)** is a 3-dimensional rendering the WPU-5 film showing the terraced nanostructure in more detail. A cross-sectional analysis was performed to measure both the step-height of the layers as well as their lateral extent. Figure 7**(b)** includes a representative cross section and the corresponding scan lines as insets. From this analysis it was determined that the step-height is approximately 5 nm per layer and on the order of several hundred nanometers laterally.

Synchrotron Analysis of WPU Films

We performed synchrotron-based SAXS and WAXS measurements on the WPU films. These measurements, conducted simultaneously, provide different aspects of structural information. Specifically, the SAXS measurements offer insights into the morphology and microstructure of the WPU films, whereas the WAXS measurements are highly sensitive to material crystallinity.

Figure 8 shows the synchrotron SAXS data. This data spans a q range that encompasses both the meso-structure and the molecular structure of the WPU films. The dashed line and arrows indicate the q ranges pertinent to each

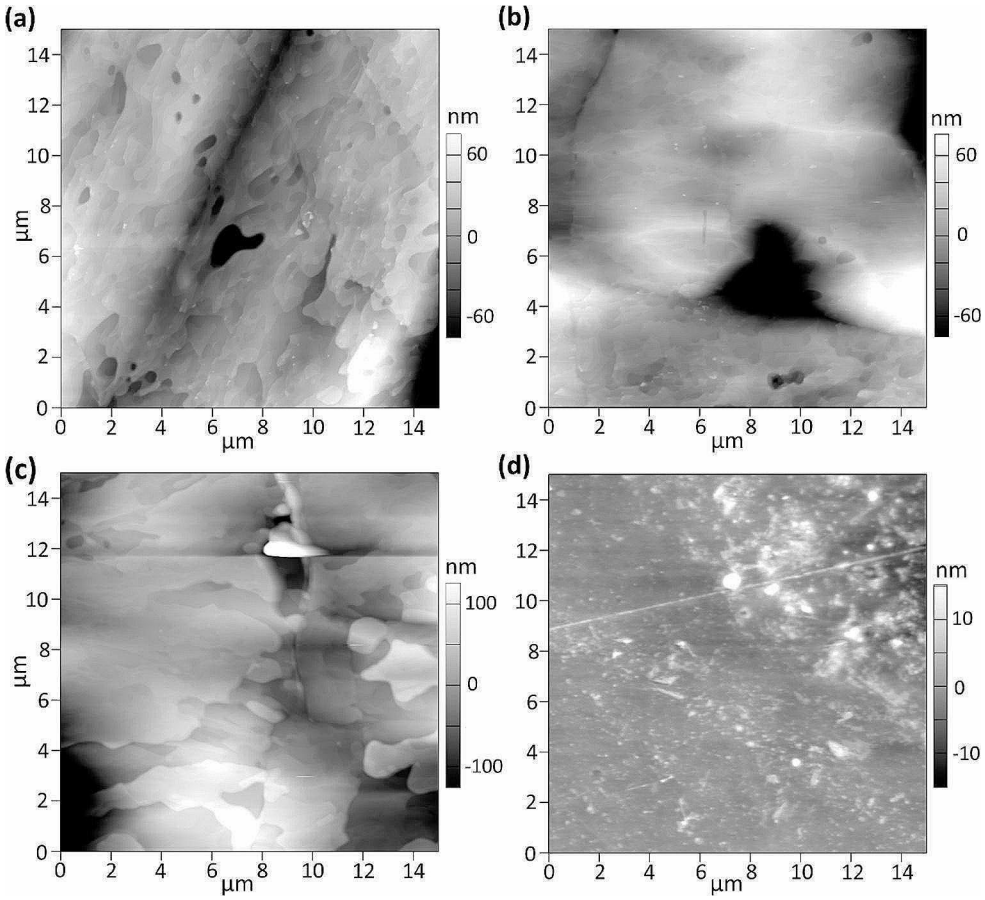

Fig. 6 AFM 15 μm × 15 μm topographic images of **a** the WPU-5 sample, **b** WPU-4 sample, **c** WPU-2 sample, and **d** the SOP/MDEA/IPDI melt cast film. The relative Z-scales are shown in nm

structure: the region pointed out by the orange arrow corresponds to the meso-structure, while the blue arrow points to the molecular structure. Here, we note that the diffuse peaks (≈ 0.27 Å^{-1} and ≈ 0.55 Å^{-1}) in the blue-arrowed region have similar peak positions, reflecting a lack of long-range order in the materials at the average separation distances related to these peaks (23.3 Å and 11.4 Å).

To elucidate the meso-structure, we conducted a SAXS analysis using Irena [29], a comprehensive SAS scattering analysis software suite. We applied a two-component model, analogous to the one developed for thermoplastic polyurethane [30–33]. Figure 9 illustrates this model. The first component represents a low-q power-law curve, suggesting the existence of large structure that SAXS alone cannot fully discern due to its detection limit (maximum detectable size ≈ 180 nm associated with a minimum $q \approx 0.0035$ Å^{-1}). The second component captures the scattering signal ranging from approximately 0.03 Å^{-1} to 0.2 Å^{-1}, pointing to the presence of a nanoscale feature. The model aligns well with the observed data, as evidenced by the agreement between the data points and the model's fit. Relevant parameters derived from this model can be found in Table 3.

The power-law exponent for all three samples ranges between -3.03 and -3.62. In SAXS analysis, this exponent typically falls between -3 and -4. It corresponds to the surface roughness of the scattering features: -4 signifies a smooth surface, while values greater than -4 indicate increasing roughness (the higher the exponent, the greater the surface roughness). Such roughness is visually evident in the AFM data in Figs. 6 and 7. We note that the AFM data are limited to the probing surface area, while the SAXS results are more statistically significant and representative. Their corroboration clearly demonstrates that the rough surface/interface exists in these WPUs.

In the context of the WPU, the scattering data implies that as the HS increases, the surface roughness of the scattering objects also increases. The nanostructures that give rise to the second scattering component has a nominal size between 154 Å and 20 Å. Connecting the AFM results and the SAXS results, a physical picture emerges. At the nanoscopic scale, the PU films exhibit a terraced structure, where each terrace has a lateral dimension of hundreds of nm and a step size of several nm to tens of nm. Coincidentally, the nominal PU particle size in the water dispersion ranges from 40 nm to 80 nm, leading to each "terrace" consisting of the volume of several PU particles. This type of hierarchical structure with two distinct lateral dimensions was also observed in WPUs with a peptide extender [34]. One possible mechanism for

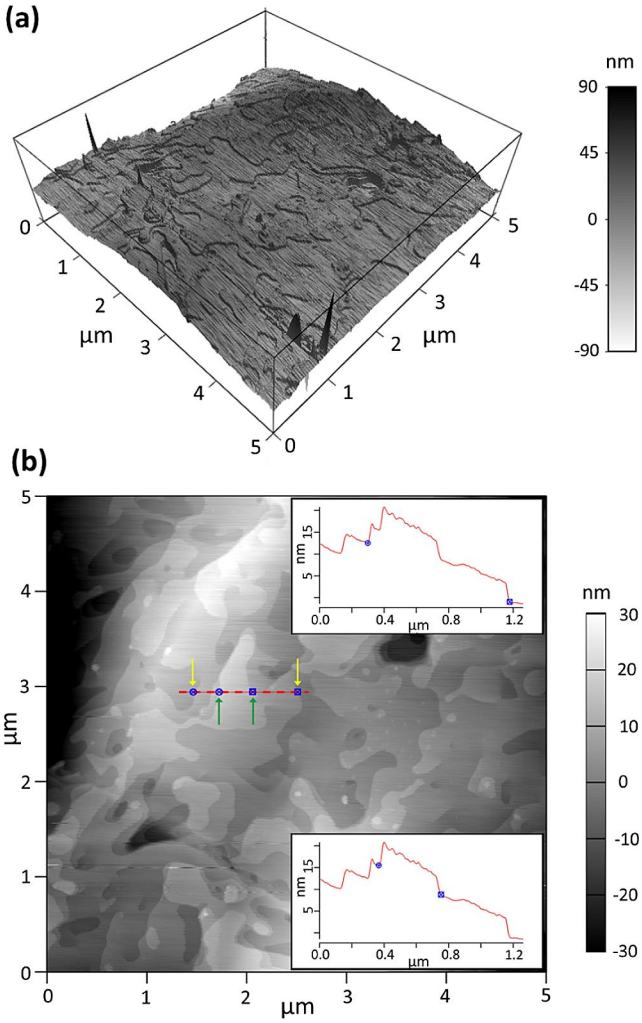

Fig. 7 **a** 5 µm × 5 µm 3D rendered AFM image of the WPU-5 film showing the terraced nanostructure. **b** the 2D AFM image shown above with a representative cross-sectional slice used to determine the step-height of 5 nm per layer and extending 386 nm (green arrows) and 880 nm (yellow arrows), respectively

Table 3 Summary of the synchrotron-based SAXS analysis of three representative WPU films

Sample Identifier	Power-law exponent	Nominal size of the nanostructure (Å)
WPU- 1	− 3.62 ± 0.05	154 ± 10
WPU-3	− 3.26 ± 0.08	21 ± 3
WPU- 5	− 3.03 ± 0.04	20 ± 2

this type of structure is through phase separation. Phase separation is affected by the molecular weight of both phases and the polarity differences as expressed in their solubility parameters [35]. Whereas soft and hard segments could be partially or completely miscible at low molar masses even with considerable differences in their solubility parameters, high molar masses certainly provide a significant driving

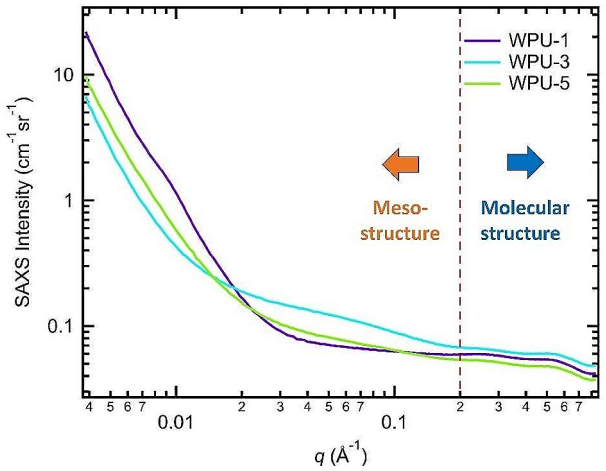

Fig. 8 Synchrotron-based small angle scattering data of three WPU samples with different HS content. The dashed line and arrows serve solely for visual guidance

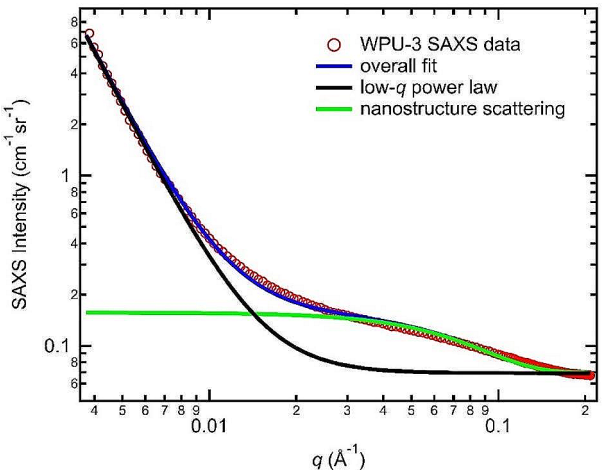

Fig. 9 An illustration of the two-component SAXS model. The model includes a power-law component originating from a size that exceeds the detection limit of the instrument, and a second component depicting a nanostructure

force for the phase separation. The calculated solubility parameter (δ) from the group contribution method, using Hoy values for the hard (IPDI/MDA) block, was 26.6 MPa$^{1/2}$ at a density of 1.10 g/cm^3 [36]. The value of δ for the polyol soft segment was estimated to be 16.7 MPa$^{1/2}$ at a density of 1.0 g/cm^3. While solubility parameters are crude predictors of physical properties and their determination depends on the chosen method of calculation, they are still useful indicators. The difference in the solubility parameters of the hard and soft segments in our case is approximately 10 MPa$^{1/2}$, which exceeds the estimated threshold difference of 2 to 4 MPa$^{1/2}$ for phase separation to occur [37]. Hence, it is logical to assume that the hard and soft segments in our WPUs underwent phase separation, which contributed to the terraced microstructure.

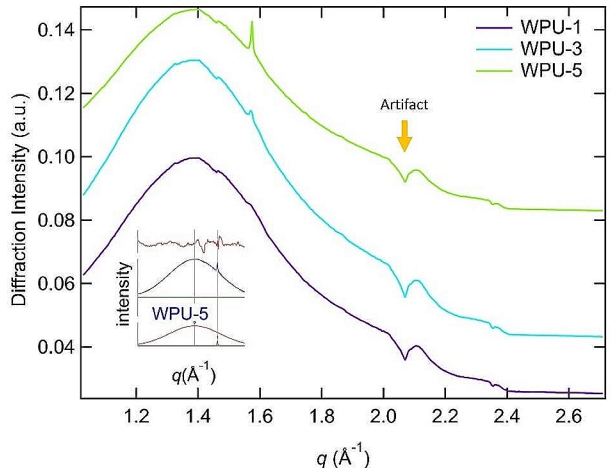

Fig. 10 Synchrotron-based wide-angle X-ray scattering data of the WPU films with three HS contents. The blue oval circle highlights the presence of a minor, but sharp diffraction peak. The dip highlighted by the read oval is an instrumental artifact. The inset shows a detailed peak profile analysis

Figure 10 shows the WAXS data. While the data primarily indicates an amorphous nature, a distinct, sharp peak appears around 1.6 $Å^{-1}$. Multiple tests conducted using different instruments, such as the WAXS component of the USAXS instrument and 12-ID WAXS, confirmed the presence of this diffraction peak. We performed a peak profile analysis on the data, incorporating both a diffuse peak and a sharp diffraction peak (as illustrated in the inset of Fig. 10). This analysis allowed us to determine the exact location and intensity of the diffraction peaks. Using these peak intensities, we assessed the crystallinity of the WPU, and the findings are compiled in Table 4. In essence, the peak's position is not significantly influenced by the HS content. While the crystallinity remains notably low, it shows a consistent relationship to the HSC: as the HS content increases, so does the crystallinity. Contrasting this with the DSC data, which implies that the hard segments of the WPU is entirely amorphous, the WAXS data, given the exceptional detection sensitivity of synchrotron-based WAXS measurements, suggest that the HS content can still possess long-range order, although to a very limited extent.

Analysis of Polymer Network Parameters

The network parameters, such as the gel point and the sol fraction, are important to understand and optimize the properties of the polyurethanes. To assess these parameters, we used the gelation theory as described in literature [38]. This theory predicts the degree of conversion at the gel point and the sol fraction in the finished network for the given input of starting materials. Also, it provides the crosslinking density expressed as the molar mass of network chains, M_c, and rubbery shear modulus. Both the input parameters and the predicted parameters are shown in Table 5.

For the WPUs with varying MDEA content, the gel points, p_c, were predicted at a conversion ratio between 0.82 and 0.86, with a higher MDEA wt% leading to a higher p_c value. The sol fractions were negligible. The calculated molar masses of ideal network chains, M_c, were in the 1366 to 1714 range. Since a network chain in a trifunctional network consists of two branches of a polyol (M = 657) and a hard segment (M = 341n + 222) then the number of repeating units, n, in the hard segments varies between 1.4 and 2.5. That is also the number of MDEA units in the hard segment, i.e., these hard segments in the ideal case are short. Shear moduli of ≈ 1.5 MPa are characteristic of soft elastomers. It must be noted, however, that these calculations did not take into account phase separation and morphology of the networks. These calculated properties serve as the basis for ideal network formations using the input (synthesis)

Table 4 Summary of synchrotron based WAXS analysis of the WPU films

Sample Identifier	Diffuse peak location (Å)	Diffuse peak intensity	Sharp peak Location (Å)	Sharp peak intensity	Estimated Crystallinity
WPU- 1	1.380	0.286	1.578	0.000336	0.0011
WPU- 3	1.376	0.337	1.573	0.000431	0.0013
WPU- 5	1.378	0.245	1.574	0.000769	0.0031

Table 5 Polyurethane network parameters calculated from the gelation theory, using input parameters of *M(SOP) = 1011 g/mol, f = 3; M(MDEA) = 119 g/mol, f = 2; M(IPDI) = 222 g/mol; f = 2*

Sample	SOP mols	MDEA mols	IPDI mols	*r* = OH/NCO ratio	$p_{c(gel)}$	*SF %	M_c g/mol	G** MPa
WPUD-1	0.3333	0.45	0.975	0.98	0.82	0.07	1366	1.81
WPUD-2	0.3333	0.5	1.025	0.98	0.82	0.08	1414	1.75
WPUD-3	*0.3333*	*0.6*	*1.125*	*0.98*	*0.84*	*0.04*	*1510*	*1.68*
WPUD-4	*0.3333*	*0.7*	*1.23*	*0.98*	*0.86*	*0.13*	*1612*	*1.54*
WPUD-5	*0.3333*	*0.8*	*1.33*	*0.98*	*0.86*	*0.16*	*1714*	*1.45*

**Sol fraction at full conversion* ($p = 1$)

***Shear modulus.*

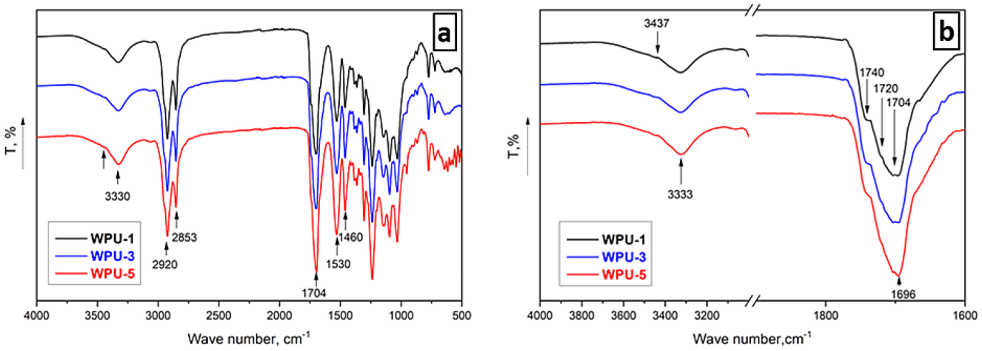

Fig. 11 **a** FTIR spectra of the cast WPU-films and **b** selected magnified spectra associated with O-H/N-H and carbonyl bands

conditions. Any discrepancy between experimental values, as shown later in the paper, and these theoretical predictions highlights the imperfections of the actual synthesis process.

Properties of WPU cast Films

Films created from the WPU dispersions were cast into Teflon molds. Once set, the cured PU films underwent a series of analysis, including FTIR, DSC, DMA, tensile tests, water absorption and water contact angle, to evaluate their properties such as chemical composition, thermal, mechanical, and hydrophobic properties.

Figure 11 presents the FTIR spectra of selected WPU films (WPU-1, 3, and 5). We observed the PU characteristic absorption peaks at 3325 cm^{-1}, 1704 cm^{-1}, and 1530 cm^{-1}, attributed to the hydrogen bonded - NH stretching vibration, -C = O stretching vibration, and -NH bending vibration, respectively [15, 39]. A small shoulder peak at 3437 cm^{-1} is associated with the non-bonded N-H stretching vibration. In addition, the absorption peaks at 2920 cm^{-1}, 2850 cm^{-1}, and 1460 cm^{-1} correspond to the C-H stretching of the $-CH_2$ and $-CH_3$ groups. The coupling absorption of the stretching vibration of C-N and in-plane deformation vibration of N-H is observed at 1530 cm^{-1}. This peak is the characteristic absorption of a quaternary ammonium salt [40].

A strong peak at ≈3330 cm^{-1}, which is attributed to the hydrogen-bonded N-H stretching vibrations, and a small shoulder peak at 3437 cm^{-1} that indicates non-H-bonded N-H stretching confirm that most amide groups are involved in hydrogen bonding. The peak at 1740 cm^{-1} is associated with the free C = O stretching, while the peaks at 1720 cm^{-1} and 1704 cm^{-1} are due to hydrogen-bonded C = O stretching predominately located within the disordered region [15]. Additionally, the peaks at 1684 cm^{-1} to 1702 cm^{-1}, indicating C = O stretching band characteristic for hydrogen bonds in the ordered or crystalline regions, are notably absent. Such evidence indicates that the prepared WPUs are overwhelmingly amorphous, in excellent agreement with the synchrotron WAXS results where only less than 0.3% of the material is found to be crystalline.

Table 6 Properties of WPU-cast films and two melt-cast reference films

Sample	MDEA, wt%	24 h water absorption %	* WCA degree	** Volume swelling (V/V_o)	Sol fraction, after 48 h in DMF, %
[a]SOP/IPDI	0	0.3	92 ± 2.2	2.1	0.7
[a]SOP/	11.6	1.8 ± 0.3	85 ± 3.6	(2.7***)	(1.6***)
MDEA/	8.3	2 ± 0.1	88 ± 2.9	2.01***	1.13 ± 0.5
IPDI	9.0	3 ± 0.8	87 ± 3.7	5.9	23.3 ± 0.4
WPU-1				6.6	28.0 ± 0.7
WPU-2					
WPU-3	10.3	3 ± 0.5	89 ± 7.4	10.5	47.6 ± 1.6
WPU-4	11.5	3 ± 0.6	89 ± 4.7	8.9	41.2 ± 0.3
WPU-5	12.5	3 ± 0.4	85 ± 2.1	–	61.4 ± 3.1

* Water contact angle on films deposited on glass

**Swelling degree in DMF after 24 h

***in toluene

[a] Melt cast films without acetic neutralization

Using a standard gravimetric method, we characterized the water adsorption of the WPU samples, as well as two melt-cast reference films. These measurements show that the WPU films typically absorb ≈ 3 wt % water after 24 h immersion (Table 6). The water contact angles (WCA) of the WPU films (cast from dispersions on glass slides) ranged from 87° to 89°. The high contact angle and low water absorption show that these films are highly hydrophobic despite the presence of ionic groups. This characteristic is attributed to the hydrophobic nature of the soft segments.

The WPU films demonstrated a significant swelling ratio, ranging from 5.9 to 10.5, upon immersion in DMF. The degree of swelling of WPU films is mainly influenced by the MDEA content and by cross-linking density [39]. Similarly, the sol fractions of these WPUs, after immersion in DMF for 48 h, are remarkably high, exceeding 61% in the case of WPU-5, which has the highest MDEA content, again suggesting poor cross-linking (incomplete crosslinking reaction and low crosslinking density).

To rationalize this lack of crosslinking, we compared the actual, measured sol fraction with an ideal SOP-MDEA-IPDI network with 50% HSC. Figure 12 shows the theoretical sol fraction dependence on the conversion ratio for such

an ideal polymer network. Evidently, at conversions above the gel point (≈86%), the sol fraction decreases exponentially. For example, the predicted sol fractions at 88% and 92% conversions are 57% and 18%, respectively. Comparing these values with the experimental sol fractions presented in Table 6 leads us to conclude that the conversion of the OH group in the WPU samples did not exceed 92%, while all the NCO groups were consumed in side reactions and were not detected by FTIR.

In contrast to the WPU films, the reference SOP/IPDI and SOP/MDEA/IPDI films, which were cast from the bulk mixture, compare favorably with the ideal networks with their low sol fractions (and limited degree of swelling). All evidence points to an incomplete reaction for the WPU films, partly because of the early dispersion in water and side reactions in the dispersed droplets. Therefore, WPU polyurethanes are comprised of mixtures of non-crosslinked branched and crosslinked molecules. The imperfection of networks, correlating with the sol fraction, significantly influences the film formation and properties of polymers, in addition to the number of ionic groups and HSC.

Film Formation from Waterborne PU Dispersions

At this juncture, it may be appropriate to examine the mechanism of film formation from dispersions. The liquid polymerization mass contains MEK as solvent before gelation. When dispersed in water, such mass essentially forms an emulsion of liquid (polymer with some solvent). A portion of the MEK solvent diffuses into the water. The reaction between IPDI and polyol/ MDEA proceeds independently within each particle, leading to the formation of solid nanoparticles. The process is partially compromised by NCO-water reactions and the subsequent amine-NCO reactions, resulting in imperfect polymer networks having unreacted OH groups and partially reacted species that are soluble in toluene and DMF.

A kinetic aspect of the synthesis also exists. If the dispersion is cast in a mold shortly after its preparation, it can yield different results (softer particles) compared to casting after a longer period, when all the NCO groups have reacted to a higher degree. During curing, as the water evaporates, the concentration of the PU particles increases and eventually the particles begin to make physical contact. The imperfect networks and soluble oligomers may promote the chemical crosslinking reactions and help coalescence of nanoparticles as observed in emulsions [41]. The reaction, although not entirely complete even after all NCO is consumed, can benefit from the interdiffusion of species for coalescence. The resulting films may show no evidence of individual nanoparticles by AFM if the films are processed in the rubbery state (above T_g of the polymer), as our AFM results clearly demonstrate. Particle aggregates may form due to ion-ion interactions, various hydrogen bonds, and ion/hydrogen bonds, as observed in our X-ray scattering and AFM analyses, leading to the formation of structures with multiple levels of heterogeneity, irrespective of the quality of the film formation. [42]

In essence, film formation from casting WPU dispersion involves water evaporation and the coalescence of nanoparticles bound by electrostatic bonds, whereas casting from the reaction mixture results in a homogeneous film held together solely by covalent bonds.

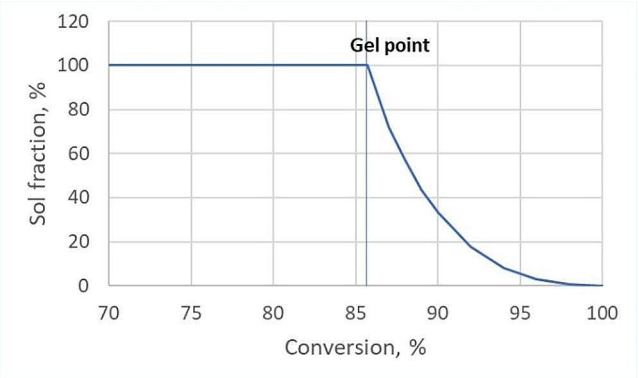

Fig. 12 Theoretical dependence of the sol fraction on the conversion ratio for a SOP-MDEA-IPDI polymer network with 50% HSC.

Table 7 Thermal and mechanical properties of the WPU films and reference cast films from the DSC and tensile tests

Sample	*HSC, wt%	MDEA, wt%	T_g, °C (DSC)	Tensile strength, MPa	Elongation at break, %
SOP/IPDI	0 (24**)	0	7	3.4 ± 0.5	178 ± 17
SOP/MDEA/IPDI	50	11.6	33	10.9 ± 1.4	187 ± 35
WPU-1	42.1	8.3	11	6.8 ± 0.4	444 ± 65
WPU-2	43.6	9.0	13	5.1 ± 0.8	361 ± 31
WPU-3	46.4	10.3	13	4.3 ± 0.4	356 ± 24
WPU- 4	49.0	11.5	21	8.1 ± 0.3	301 ± 26
WPU-5	51.3	12.5	20	6.2 ± 0.5	260 ± 30

*Hard segment concentration (IPDI + MDEA), **IPDI content

Thermal and Mechanical Properties

DSC curves of the WPU cast films display a single T_g between 11 °C and 21 °C (see Supplemental Information). Table 7 demonstrates that, with increasing the HSC from 42 to 51% and the number of the ionic groups, the T_g of the WPU films increases, too. The T_g of the pure hard segment is ≈77 °C, and for the IPDI/SOP copolymer, it is ≈7 °C. The singular T_g of the WPU samples and the absence of distinct glass transitions for the hard and soft phases suggest a lack of clear phase separation. This may be attributed to

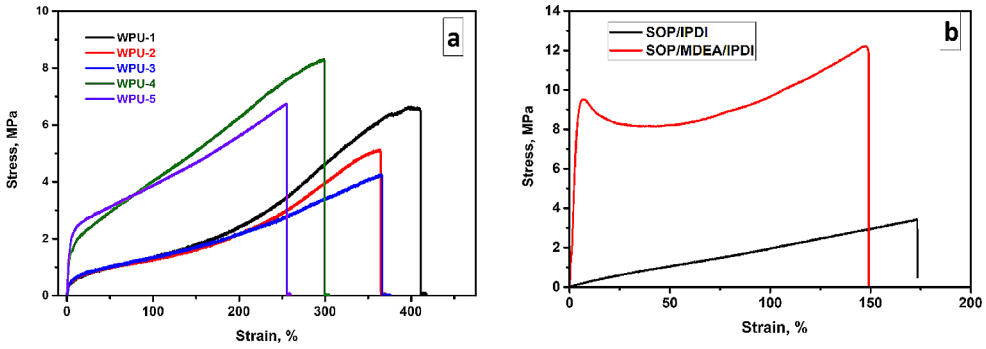

Fig. 13 Stress-strain curves for the WPU films (a) and melt cast SOP/IPDI and SOP/MDEA/IPDI films (b)

Table 8 DMA analysis results of WPU films

Sample	HSC, wt%	MDEA, wt%	E′ (-80 °C) MPa	E" (-80 °C) MPa	α, °C $(G'')_{peak}$	α, °C $(\tan\delta)_{peak}$	β, °C $(\tan\delta)_{peak}$
WPU-1	42.1	8.3	6212	0.281	13	34	< − 100
WPU-2	43.6	9.0	7700	0.248	16	38	
WPU-3	46.4	10.3	1279	0.172	18	36	~ − 100
WPU-4	49.0	11.5	5463	0.081	21	42	− 75
WPU-5	51.3	12.5	4356	0.064	21	40	− 40

the relatively low molar mass and the amorphous nature of the hard segments, possibly small domain sizes, and interactions between phases, serving to hinder a clear microphase separation. In addition, the agglomeration of ionic centers would affect the final morphology and shift the T_g to higher values. The diffusion of ionic centers to the surface of nanoparticles is impeded by crosslinks, making it improbable for all ionic groups to be located in the outer shell. This may explain why the required number of ionic groups for a stable dispersion is relatively high, compared to with some anionic systems [18, 43, 44], although it must be acknowledged that such a requirement would be dependent on the structure and polarity of the polyol.

Stress-strain test results, as illustrated in Fig. 13a and b and listed in Table 7 are typical for elastomers. Stress increases at high elongations, resembling stress-induced crystallization in rubbers, and this may be explained by aligning the chains and improving ionic center association. The curves of WPU-1, WPU-2 and WPU-3 films exhibit tensile strengths of 4.3 MPa to 6.8 MPa, and an elongation at break of 360–440%. WPU-1 film, which has the lowest hard segment and MDEA content, the lowest sol fraction and lowest T_g, shows the highest elongation but also a relatively high strength, demonstrating the effectiveness of improved network structure. An increase in the HSC, and more importantly, the ionic group content, leads to increased strengths and moduli but reduced elongations. In comparison, the non-ionic SOP-IPDI cast reference material with a better network structure but no hard segments, displayed the lowest T_g, tensile strength and elongation, as listed in Table 7. Meanwhile, the ionic SOP/MDEA/IPDI cast reference material (without solvent and not from dispersion in water) showed a T_g of 33.2 °C, a tensile strength of 10.9 MPa, and an elongation of 187%. In other words, the incorporation of the ionic hard segments leads to the increase of the T_g and the tensile strength for conventional cast PU films.

We also evaluated the effect of using acetic acid to neutralize the reactive groups of SOP/MDEA/IPDI during traditional casting. Acetic acid caused a foaming reaction with the SOP/MDEA/IPDI, making good neutralized polymer samples for mechanical testing unavailable. The T_g of the neutralized film was found to be ≈ 26 °C, i.e., neutralization did not enhance T_g. The impact of the degree of neutralization in anionic films has been reported to yield optimal properties at the stoichiometric ratio [45].

The viscoelastic behavior of the cast WPU films was analyzed by DMA in tensile mode at 1 Hz. Table 8 shows the storage and loss moduli at -80 °C and 80 °C. Figure 14 shows the storage modulus (E') and tan δ as a function of temperature. The α-transition temperature (T_g) was acquired at the maximum of the tan δ and E'' for each curve. E' values in the glassy state are in the GPa region and drop precipitously several orders of magnitude in the transition region, but never reach a plateau in the measured temperature range. The lowest moduli were considerably below the calculated values of ≈ 1.5 MPa (see Table 5), as predicted by rubber elasticity theory, pointing to low conversions during synthesis and poor cross-linking.

α-Transitions, associated with cooperative segmental motions in the networks, were identified as the maxima on E''-temperature curves between 16 °C and 21 °C, and on tan δ curves from 34 °C to 42 °C at a frequency of 1 Hz. Clearly defined β-transitions, observed around − 40 °C, are associated with rotational motions of some unidentified

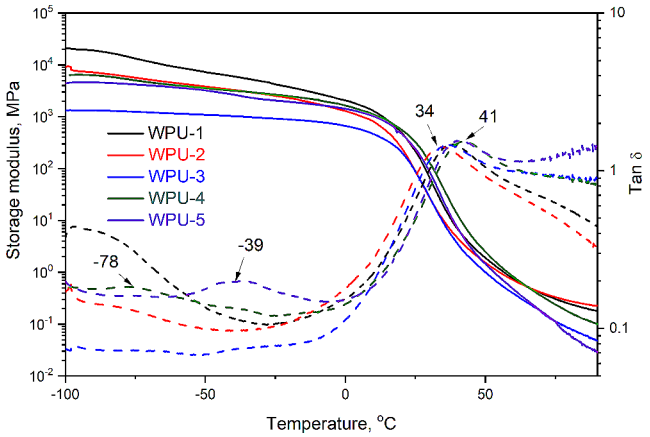

Fig. 14 Temperature-dependent storage modulus (E') and tan δ for the WPU films

small groups in the polymer chains Specifically, these β-transitions temperatures were − 40 °C and − 75 °C for WPU-5 and WPU-4, respectively. The β-transition temperatures were assumed to be below − 100 ° C for WPU-1 and WPU-2. β-Transitions appear to be correlated with the concentration and possibly the size of ionic aggregates, shifting to higher temperatures with increasing ionic strength.

Thermal stability of WPU films was evaluated by TGA in a nitrogen environment. The TGA and DTG curves of WPU films with different content of MDEA or HS, as well as that of the pure hard segment are shown in the Supplement Info (**Fig. S6)**. The onset of degradation, taken as 5% loss ($T_{5\%}$), was at ≈250 °C. DTG shows two stages in the thermal degradation process [39]. In the first stage, the labile urethane bonds in the hard segments of polymer chains were decomposed with the maximum degradation rate at temperatures between 307 °C and 317 °C. The second stage is dominated by the degradation of SOP polyol with its maximum rate between 365 °C and 371 °C. The data also clearly demonstrate that, as the content of HS in WPU films increased, the thermal stability of the prepared films decreased.

Conclusions

The preparation of water dispersions of cross-linkable cationic polyurethanes with bio-content above 50%, utilizing high oleic soybean oil, was successfully carried out. The degree of crosslinking is influenced by the preparation method and the presence of water, resulting in imperfect networks. The lower functionality and more regular structure of high oleic soybean oil, compared to standard soybean oil, allowed higher conversions of functional groups before gelation. A comprehensive structural analysis of high oleic soybean oil, polyol, and the pure hard segment improved our understanding of the structure of polyurethane films. The average particle size of the polyurethane dispersion ranged between 38 nm and 68 nm and decreased with increasing ionic group content. The ionic strength was sufficient for stable dispersion while maintaining low particle size.

Analysis of the polymer networks through swelling and soluble fraction measurements showed that the formation of imperfect networks was the result of side reaction with water after dispersion. The resulting coatings exhibited relatively good strengths, which increased with the ionic content. DMA studies revealed that the transition temperatures of α-, and particularly, β-transitions rose with increasing ionic group content.

AFM and synchrotron analyses of WPU films reveal distinct morphological and structural characteristics. The AFM data showed WPU films exhibit a terraced nanostructure with layers approximately 5 nm in height and several hundred nanometers laterally, differing significantly from smoother, previously investigated films. Synchrotron-based SAXS and WAXS measurements provided insights into the films' microstructure and material crystallinity, indicating an increase in surface roughness and nominal nanostructure size with higher hard segment content, and a slight increase in crystallinity despite the predominantly amorphous nature of the hard segments. These findings suggest a complex interplay of phase separation and material composition in determining WPU film morphology and structure.

Despite the relatively high ionic group content, the synthesize films containing vegetable oil soft segment exhibited low water absorption of around 3%, and contact angles of around 90°, indicating good hydrophobicity and the potential for applications in textile and leather protective coatings.

Supplementary Information The online version contains supplementary material available at https://doi.org/10.1007/s10924-024-03368-5.

Acknowledgements We are indebted to the Kansas Soybean Commission for financial support. This research used resources of the Advanced Photon Source, a U.S. Department of Energy (DOE) Office of Science user facility at Argonne National Laboratory and is based on research supported by the U.S. DOE Office of Science-Basic Energy Sciences, under Contract No. DE-AC02-06CH11357. We would also like to thank Prof. Richard Weiss of the Georgetown University for discussions.

Author Contributions Zoran Petrović: Formal analysis, Investigation, Methodology, Visualization, Writing – original draft, Conceptualization, Funding Acquisition. Jasna Djonlagić: Formal analysis, Investigation, Methodology, Visualization, Writing – review & editing. Jian Hong: Formal analysis, Investigation, Methodology, Visualization, Writing – review & editing. Milica Lovrić Vuković: Formal analysis, Investigation, Methodology, Visualization, Writing – review & editing. Jan Ilavsky: Investigation, Methodology, Visualization, Writing – review & editing. Brian G. Bush: Formal analysis, Investigation, Methodology, Visualization, Writing – review & editing. Fan Zhang: Formal analysis, Investigation, Methodology, Visualization, Writing – original draft.

Funding Open access funding provided by the National Institutes of Health.

Data Availability Data is provided within the manuscript or supplementary information files and is available upon request.

Declarations

Competing Interests The authors declare no competing interests.

References

1. Dieterich D (1981) Aqueous emulsions, dispersions and solutions of polyurethanes; synthesis and properties. Prog Org Coat 9(3):281–340
2. Petrović ZS, Ferguson J (1991) Polyurethane elastomers. Prog Polym Sci 16(5):695–836
3. Garrett JT, Siedlecki CA, Runt J (2001) Microdomain morphology of poly (urethane urea) multiblock copolymers. Macromolecules 34(20):7066–7070
4. Tocha E, Janik H, Debowski M, Vancso GJ (2002) Morphology of polyurethanes revisited by complementary AFM and TEM. J Macromolecular Sci Part B 41(4–6):1291–1304
5. Li C, Goodman SL, Albrecht RM, Cooper SL (1988) Morphology of segmented polybutadiene-polyurethane elastomers. Macromolecules 21(8):2367–2375
6. Yilgör I, Yilgör E, Wilkes GL (2015) Critical parameters in designing segmented polyurethanes and their effect on morphology and properties: a comprehensive review. Polymer 58:A1–A36
7. Xiao H, Frisch K (1995) Advances in urethane Ionomers., Inc. Technomic Publishing Company Inc., Lancaster, Pennsylvania, USA
8. Zhang L, Brostowitz NR, Cavicchi KA, Weiss R (2014) Perspective: Ionomer research and applications. Macromol React Eng 8(2):81–99
9. Khranovskii V, Lipatov YS, Maslyuk A, Yatsimirskaya T, Bereznitskii G (1987) Study of intermolecular interactions in cation-containing oligo-urethanes with a different chemical nature of the anion. Polym Sci USSR 29(6):1285–1293
10. Petrović ZS (2008) Polyurethanes from vegetable oils. Polym Rev 48(1):109–155
11. Ono HK, Jones FN, Pappas SP (1985) Relative reactivity of isocyanate groups of isophorone diisocyanate. Unexpected high reactivity of the secondary isocyanate group. J Polym Science: Polym Lett Ed 23(10):509–515
12. Delebecq E, Pascault J-P, Boutevin B, Ganachaud F (2013) On the versatility of urethane/urea bonds: reversibility, blocked isocyanate, and non-isocyanate polyurethane. Chem Rev 113(1):80–118
13. Lomölder R, Plogmann F, Speier P (1997) Selectivity of isophorone diisocyanate in the urethane reaction influence of temperature, catalysis, and reaction partners. J Coatings Technol 69(868):51–57
14. Kapp R (2014) In: Wexler P (ed) Isocyanates, Encyclopedia of Toxicology. Third Edition), Ed, pp 1112–1131
15. Lu Y, Larock RC (2008) Soybean-oil-based waterborne polyurethane dispersions: effects of polyol functionality and hard segment content on properties. Biomacromolecules 9(11):3332–3340
16. Barni A, Levi M (2003) Aqueous polyurethane dispersions: a comparative study of polymerization processes. J Appl Polym Sci 88(3):716–723
17. Zhou X, Fang C, Lei W, Du J, Huang T, Li Y, Cheng Y (2016) Various nanoparticle morphologies and surface properties of waterborne polyurethane controlled by water. Sci Rep 6(1):34574
18. Santamaria-Echart A, Fernandes I, Barreiro F, Corcuera MA, Eceiza A (2021) Advances in waterborne polyurethane and polyurethane-urea dispersions and their eco-friendly derivatives: a review. Polymers 13(3):409
19. Duan J, Jiang G (2022) Synthesis, characterization and properties of antibacterial polyurethanes. Polymers 14(1):213
20. Kim B (1996) Aqueous polyurethane dispersions. Colloid Polym Sci 274:599–611
21. Flider FJ (2021) High oleic oils: Development, Properties, and uses. Elsevier
22. Ilavsky J, Zhang F, Andrews RN, Kuzmenko I, Jemian PR, Levine LE, Allen AJ (2018) Development of combined microstructure and structure characterization facility for in situ and operando studies at the Advanced Photon source. J Appl Crystallogr 51(3):867–882
23. Zhang F, Allen AJ, Levine LE, Vaudin MD, Skrtic D, Antonucci JM, Hoffman KM, Giuseppetti AA, Ilavsky J (2014) Structural and dynamical studies of acid-mediated conversion in amorphous-calcium-phosphate based dental composites. Dent Mater 30(10):1113–1125
24. Zhang F, Ilavsky J (2010) Ultra-small-angle X-ray scattering of polymers. J Macromolecular Science® Part C: Polym Reviews 50(1):59–90
25. Petrović ZS, Zlatanić A, Lava CC, Sinadinović-Fišer S (2002) Epoxidation of soybean oil in toluene with peroxoacetic and peroxoformic acids—kinetics and side reactions. Eur J Lipid Sci Technol 104(5):293–299
26. Zlatanić A, Petrović ZS, Dušek K (2002) Structure and properties of triolein-based polyurethane networks. Biomacromolecules 3(5):1048–1056
27. Petrovic Z, Javni I, Guo A, Zhang W (2002) Method of making natural oil-based polyols and polyurethanes therefrom, Google Patents
28. Nimesh S, Chandra R, Gupta N (2017) Advances in nanomedicine for the delivery of therapeutic nucleic acids. Woodhead Publishing
29. Ilavsky J, Jemian PR (2009) Irena: tool suite for modeling and analysis of small-angle scattering. J Appl Crystallogr 42(2):347–353
30. Javni I, Bilić O, Bilić N, Petrović ZS, Eastwood EA, Zhang F, Ilavský J (2015) Thermoplastic polyurethanes with isosorbide chain extender. J Appl Polym Sci 132(47)
31. Javni I, Bilić O, Bilić N, Petrović ZS, Eastwood EA, Zhang F, Ilavský J (2015) Thermoplastic polyurethanes with controlled morphology based on methylenediphenyldiisocyanate/isosorbide/butanediol hard segments. Polym Int 64(11):1607–1616
32. Petrović ZS, Milić J, Zhang F, Ilavsky J (2017) Fast-responding bio-based shape memory thermoplastic polyurethanes. Polymer 121:26–37

33. Petrović ZS, Hong D, Javni I, Erina N, Zhang F, Ilavský J (2013) Phase structure in segmented polyurethanes having fatty acid-based soft segments. Polymer 54(1):372–380
34. Zhang F, Wang R, He Y, Lin W, Li Y, Shao Y, Li J, Ding M, Luo F, Tan H (2018) A biomimetic hierarchical structure with a hydrophilic surface and a hydrophobic subsurface constructed from waterborne polyurethanes containing a self-assembling peptide extender. J Mater Chem B 6(26):4326–4337
35. Van Krevelen D (1990) Cohesive properties and solubility, Properties of polymers 189–225
36. Grulke EA (2003) Solubility parameter values, The Wiley Database of Polymer Properties
37. Painter PC, Coleman MM (1997) Fundamentals of polymer science: an introductory text, (No Title)
38. Ilavský M, Dušek K (1983) The structure and elasticity of polyurethane networks: 1. Model networks of poly (oxypropylene) triols and diisocyanate. Polymer 24(8):981–990
39. Liang H, Feng Y, Lu J, Liu L, Yang Z, Luo Y, Zhang Y, Zhang C (2018) Bio-based cationic waterborne polyurethanes dispersions prepared from different vegetable oils. Ind Crops Prod 122:448–455
40. Li M, Liu F, Li Y, Qiang X (2017) Synthesis of stable cationic waterborne polyurethane with a high solid content: insight from simulation to experiment. RSC Adv 7(22):13312–13324
41. Ludwig I, Schabel W, Castaing J, Ferlin P, Kind M (2005) Film Formation from Industrial Waterborne Latices, Poceedings of the 6th European Coating Symposium (ECS), Bradford, UK
42. Overbeek A (2010) Polymer heterogeneity in waterborne coatings. J Coat Technol Res 7(1):1–21
43. Kim BK, Lee JC (1996) Waterborne polyurethanes and their properties. J Polym Sci Part A: Polym Chem 34(6):1095–1104
44. Sardon H, Irusta L, Fernández-Berridi MJ, Luna J, Lansalot M, Bourgeat-Lami E (2011) Waterborne polyurethane dispersions obtained by the acetone process: a study of colloidal features. J Appl Polym Sci 120(4):2054–2062
45. Jang JY, Jhon YK, Cheong IW, Kim JH (2002) Effect of process variables on molecular weight and mechanical properties of water-based polyurethane dispersion. Colloids Surf a 196(2–3):135–143

Authors and Affiliations

Zoran S. Petrović[1] · Jasna Djonlagić[1] · Jian Hong[1,2] · Milica Lovrić Vuković[1] · Jan Ilavsky[3] · Brian G. Bush[4] · Fan Zhang[4]

✉ Zoran S. Petrović
zpetrovic@pittstate.edu

✉ Fan Zhang
fanzhang@nist.gov

[1] Kansas Polymer Research Center, Pittsburg State University, Pittsburg, KS 66762, USA

[2] Checkerspot Inc, Alameda, CA 94501, USA

[3] X-ray Science Division, Argonne National Laboratory, 60439 Argonne, IL, USA

[4] Materials Measurement Science Division, National Institute of Standards and Technology, Gaithersburg, MD 20899, USA